Rapid Communications

Pressure-induced superconductivity in semimetallic 1*T*-$TiTe_2$ and its persistence upon decompression

U. Dutta,[1,2] P. S. Malavi,[1,*] S. Sahoo,[1] B. Joseph,[3] and S. Karmakar[1,2,†]

[1]*High Pressure & Synchrotron Radiation Physics Division, Bhabha Atomic Research Centre, Trombay, Mumbai 400085, India*

[2]*Department of Physical Sciences, Homi Bhabha National Institute, Anushaktinagar, Mumbai 400094, India*

[3]*Elettra Sincrotrone Trieste, S.S. 14, Km 163.5 in Area Science Park, Basovizza, Trieste 34012, Italy*

(Received 29 September 2017; revised manuscript received 5 December 2017; published 8 February 2018)

Pristine 1*T*-$TiTe_2$ single crystal has been studied for resistance and magnetoresistance behavior under quasihydrostatic and nonhydrostatic compressions. While the semimetallic state is retained in nearly hydrostatic pressures, small nonhydrostatic compression leads to an abrupt change in low-temperature resistance, a signature of possible charge density wave (CDW) ordering, that eventually collapses above 6.2 GPa. Superconductivity emerges at ∼5 GPa, rapidly increasing to a critical temperature (T_c) of 5.3 K at 12 GPa, irrespective of pressure condition. Pressure studies thus evidence that 1*T*-$TiTe_2$ exhibits superconductivity irrespective of the formation of the CDW-like state, implying the existence of phase-separated domains. Most surprisingly, the superconducting state persists upon decompression, establishing a novel phase diagram with suppressed P scale. The pressure quenchable superconductivity, of multiband nature and relatively high upper critical field, makes 1*T*-$TiTe_2$ unique among other layered dichalcogenides.

DOI: 10.1103/PhysRevB.97.060503

CdI_2-structured transition metal dichalcogenide compounds (e.g., 1*T*-$TiSe_2$, 1*T*-TaS_2) provide an important playground to reveal exotic ground-state electronic orders [1] by tuning the Fermi surface topology and many-body effects, either purely by lowering temperature [2–5] or by carrier doping [6–15] or applying external pressure [16–21]. The emergence of charge density wave (CDW) order at low temperature and its coexistence with superconductivity (SC) in some portion of the phase diagram have been of tremendous research interest in order to understand their origin and competitive nature [22]. The puzzling behavior of dichalcogenide SC is due to the presence of strong electron-phonon coupling and also the dome structure in the vicinity of the CDW-suppressed quantum critical point (QCP). In the BCS picture, the strong electron-phonon coupling is believed to be responsible for the emergence of both CDW and SC, where other effects such as local short-range interaction and structural disordering are able to explain the systematic suppression of CDW and SC, respectively, forming the dome structure [8,23]. On the other hand, there is an unconventional SC scenario where CDW amplitude fluctuation is believed to be responsible for the Cooper pair formation [10,18], where the relevant QCP might be near a hidden commensurate to incommensurate CDW transition [14,20].

1*T*-$TiTe_2$ is a conventional Fermi-liquid reference metal, often used to characterize the electronic structure of Cu-intercalated 1*T*-$TiSe_2$ [7,24,25]. In spite of that, only very few investigations have so far been reported on the pristine 1*T*-$TiTe_2$, particularly due to the absence of CDW order at low T [26]. In comparison with its isomorphic 1*T*-$TiSe_2$, the band structure of 1*T*-$TiTe_2$ shows enhanced indirect band overlap [having Te 5*p* hole pockets at Γ and Ti 3*d* electron pockets at the L point of the Fermi surface (FS)], characterized by semimetallic resistivity at ambient condition [25,27]. A larger Te spin-orbit interaction and enhanced *p*-*d* hybridization near Fermi level are expected to make the FS more susceptible to external parameters, such as intercalation [28], electrostatic field [29], or pressure. Indeed, recent theoretical studies have predicted that not only a suitable strain condition can induce phonon-mediated SC [30]; hydrostatic pressure and isovalent cation substitution may also lead to the emergence of nontrivial topological surface states in its bulk as well as monolayer form [31,32]. The emergence of SC in the topological surface states is of fundamental interest from the point of view of the realization of topological superconductors, hosting massless Majorana fermions.

In this Rapid Communication, we report on the transport properties of pristine 1*T*-$TiTe_2$ single crystal under various quasihydrostatic and nonhydrostatic compressions. In nearly hydrostatic condition, SC emerges at ∼5 GPa where the semimetallic positive magnetoresistance (MR) is found to decrease significantly, showing no apparent competing order in effect at FS. In contrast, application of nonhydrostatic pressure (∼1.8 GPa) leads to dramatic changes in its resistance behavior to a characteristic of quasicommensurate CDW ordered state, as seen in isomorphic 1*T*-TaS_2 [17]. With increasing pressure, this resistance anomaly gets suppressed by a systematic decrease of overall resistance and SC emerges at 6.2 GPa. T_c increases rapidly to 5.3 K up to 12 GPa, followed by a rather slow but monotonic increase up to 29 GPa, the highest pressure of this measurement. The SC state persists upon decompression at least down to 0.5 GPa, also coexisting with the reentrant CDW-like phase (as verified

*Present address: Department of Physics, Washington University in St Louis, St. Louis, MO 63130, USA.

†sdak@barc.gov.in

from our electron diffraction measurement on the P-released sample). The persistent nature of SC at almost ambient pressure upon decompression is extremely rare, but highly desirable for practical applications. The pressure-quenchable SC state will also make the surface-sensitive measurements [angle-resolved photoemission spectroscopy (ARPES)] accessible for further investigating their electronic origin and coexisting nature in this pristine compound and novel topological physics. The irreversible nature of structural evolution under nonhydrostatic compression (as demonstrated in the Supplemental Material [33]) further supports the resistance results and establishes the unique P-rescaled phase diagram.

Pristine $1T$-$TiTe_2$ single crystals in this study were grown by a conventional vapor transport method (with iodine as the transport agent) and characterized by x-ray diffraction, low-energy electron diffraction (LEED), resistivity, and magnetic susceptibility measurements [33]. The resistance was measured using a standard four-probe technique (in van der Pauw configuration), with ac lock-in detection in two different high-pressure arrangements. A Stuttgart version diamond-anvil cell (DAC) [34] was used for measurements under quasihydrostatic (up to 13 GPa) and nonhydrostatic (up to 29 GPa) pressures. In the former case, finely ground NaCl powder was used as the pressure medium. The DAC was placed inside a KONTI-IT (Cryovac) cryostat, equipped with a homemade electromagnet coil (up to 0.5 T). For high-field measurements a nonmagnetic Cu-Be DAC (easyLab) was prepared for quasihydrostatic pressures (up to 9.5 GPa) and was inserted into a S700X SQUID magnetometer (Cryogenic) to study MR up to 7 T

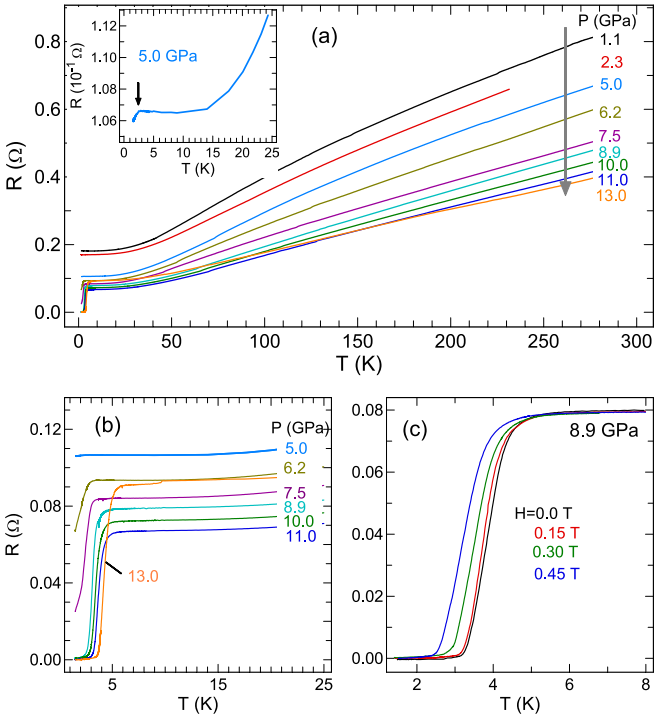

FIG. 1. (a) In-plane resistance of $1T$-$TiTe_2$ as a function of temperature at various quasihydrostatic pressures. Inset shows a significant resistance drop below SC onset T_c 2.5 K at 5 GPa. (b) The magnified R-T data near SC transition at various pressures. (c) Variation of the R-T curve near T_c under magnetic fields at 8.9 GPa.

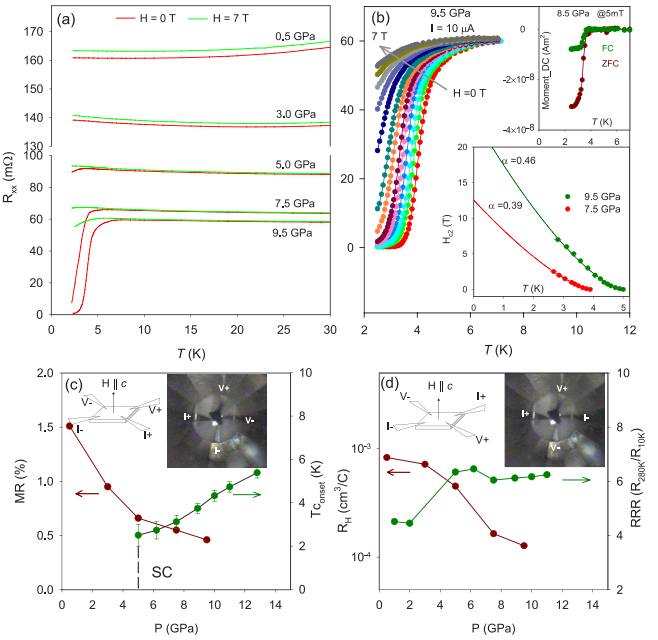

FIG. 2. (a) Low-T longitudinal resistance, measured at zero field and at 7 T, at various quasihydrostatic P. (b) $R(T)$ plots across T_c at 9.5 GPa under different fields up to 7 T. Lower inset: plots of T_c vs H at 7.5 and 9.5 GPa; solid lines are best fits using the empirical formula $H_{c2}(T) = H^*_{c2}(1 - T/T_c)^{1+\alpha}$. Upper inset: dc susceptibility of the SC state at 8.5 GPa. Plots of (c) magnetoresistance MR(%) [$=(R_{7\,\mathrm{T}}\text{-}R_{0\,\mathrm{T}}) \times 100/R_{0\,\mathrm{T}}$] at 10 K and onset T_c and (d) Hall coefficient R_H at 10 K and RRR ($=R_{280\,\mathrm{K}}/R_{10\,\mathrm{K}}$) as a function of P. Insets are schematic illustrations.

field and also dc susceptibility. P were measured by ruby luminescence.

In Fig. 1, semimetallic $R(T)$ curves at all pressures under quasihydrostatic conditions closely resemble the one at ambient P [33]. With an increase in P, the overall resistance decreases systematically, indicating an enhanced metallic character. At 5 GPa, a significant resistance drop below 2.5 K indicates the onset of SC transition [inset of Fig. 1(a)]. T_c increases monotonically [Fig. 1(b)], with $dT_c/dP = 0.35$ K/GPa. Below 7.5 GPa, SC transition is not complete at the lowest T (1.4 K) of our setup and so zero resistance is not achieved. To demonstrate that the zero resistance at higher pressures represented the SC state, we measured resistance drop at 8.9 GPa under magnetic field and found a significant decrease in T_c [Fig. 1(c)].

To understand the evolution of electronic structure exhibiting SC, we carried out magnetoresistance (MR) and Hall measurements at high P (with $H = 7$ T along the c axis). Figure 2(a) displays the effect of high field on the low-T longitudinal resistance (R_{xx}) at various hydrostatic P. The measured MR at 10 K is plotted as a function of P in Fig. 2(c). The paramagnetic semimetallic positive MR at 0.5 GPa agrees well with the reported result of stoichiometric $1T$-$TiTe_2$ at ambient pressure [35]. With increasing P, MR decreases by a factor of 3 at 5 GPa, where SC emerges. As T_c increases with P, MR gets further suppressed, but remains positive. The hole-dominated positive Hall coefficient R_H, as obtained from the measured transverse resistance (R_{xy}), also agrees well with

an earlier report [26]. R_H remains almost P independent up to 5 GPa, above which it starts decreasing rapidly [see Fig. 2(d)] showing increased effective carrier concentration, which is also supported by the observed enhanced RRR value above this P. In addition to these, the observed nonlinear H^2 dependence of MR (see Fig. S5 of the Supplemental Material [33]) across this P indicates significant changes of hole and electron bands at the FS, favoring SC to emerge.

In Fig. 2(b), we plot the field variation of $R(T)$ at 9.5 GPa around T_c. The zero resistance state (with $T_c \sim 5$ K at $H = 0$ T) is gradually lifted with increasing magnetic field, resulting in a systematic decrease in T_c. At a magnetic field of 7 T the SC transition almost smears out. In the T_c-H plot [as shown in the inset of Fig. 2(b)], a positive curvature close to $T_c(H = 0)$ clearly indicates the deviation of a single-band model of the Werthamer-Helfand-Hohenberg theory for the upper critical field $H_{c2}(T)$ [36] and suggests a need for two-band analysis, as in the case of NbS_2 and $NbSe_2$ [37,38]. The experimental data $H_{c2}(T)$, when fitted with the empirical formula [39] $H_{c2}(T) = H^*_{c2}(1 - T/T_c)^{1+\alpha}$, estimates $H^*_{c2} > 10$ T, which is larger than $2H$-$NbSe_2$ [37] and $1T$-$TiSe_2$ [18] and also higher than the BCS weak-coupling Pauli limit $H_p = 1.86 * T_c(0) \sim 9.3$ T. This is in stark contrast with other layered chalcogenides, where Pauli-limited behavior of the upper critical field has been observed [18,37,38]. However, strong spin-orbit coupling in reduced dimension or local disorder can suppress paramagnetic pair breaking effect and violate the Pauli limit by a factor of 3–6 in the case of the dirty limit of BCS SCs [40,41]. Higher field measurements at further low T are needed for better insight in this regard. Low-T resistivity data of $1T$-$TiTe_2$ gives mean free path $\lambda \sim 7$ nm [42], which is of the same order of the estimated coherence length $\xi_{GL} = \sqrt{\Phi_0/2\pi H_{c2}(0)} = 3.6$ nm and so the observed SC is of multiband BCS type, but not in the clean limit regime. With the coherence length being greater than the interplane separation, SC is of three-dimensional (3D) nature. Moreover, H_{c2} vs T_c plots at 7.5 and 9.5 GPa are in good agreement as per BCS estimation $H_{c2}(0) \propto T_c^2$. The bulk SC is also confirmed by the susceptibility measurements on pressurized samples [upper inset of Fig. 2(b)] [33].

Now we present $R(T)$ under nonhydrostatic compression. Here a thin single crystal $TiTe_2$ is placed onto the insulated gasket (without drilling a hole), without a pressure medium. Figure 3 shows in-plane $R(T)$ under various compressive pressures and upon decompression. At a small nonhydrostatic P (~1.8 GPa), the ambient semimetallic R changes abruptly into a broad humplike R-T curve with overall R increased by two orders of magnitude [Fig. 3(a)]. With increasing P, the overall R systematically decreases, but retains the hump feature up to 6.2 GPa. The hysteresis in the cooling and heating cycle of the R-T curve (shown for 6.2 GPa data) evidences the first-order transition, as observed in the $1T$-TaS_2 quasicommensurate charge density wave ordered state having phase-separated domain structures [17]. We believe the CDW-like ordering temperature is above room T. The observed low-T resistance upturn below 40 K also gets suppressed along with the hump, indicating superstructure-related localization being its origin. The broad R hump moves to higher T (as shown by its characteristic temperature T^*) as P increases to 3.7 GPa. Above this pressure, T^* decreases before the feature gets unresolved above 6.4 GPa, while the unconventional

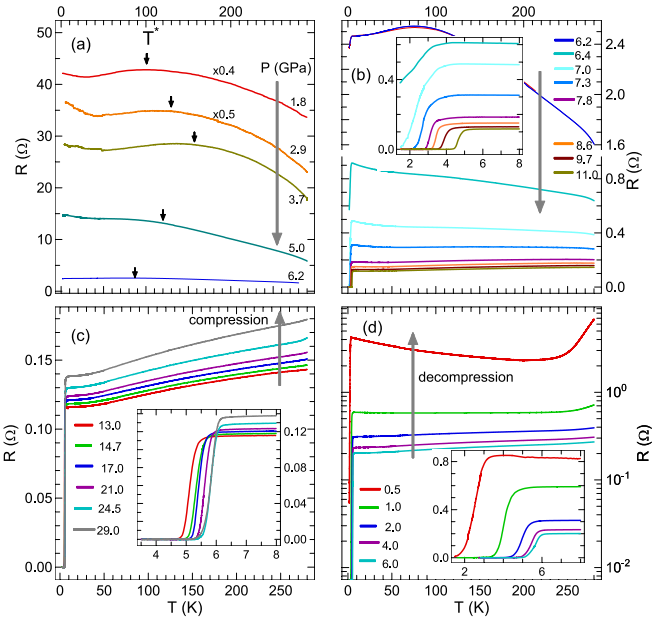

FIG. 3. Temperature-dependent in-plane resistance of $1T$-$TiTe_2$ single crystal under (a)–(c) various nonhydrostatic compression up to 29 GPa and (d) decompression pressures. Insets in respective panels show magnified R-T data near superconducting transitions at various pressures.

metallic behavior ($dR/dT < 0$) persists up to ~8.6 GPa [Fig. 3(b)]. A sharp resistance drop indicating SC onset is observed at 6.2 GPa, although a complete zero resistance is seen only above 7 GPa. T_c increases with increasing P at the same rate of hydrostatic compression. At higher P the system enters into conventional metallic regime (with $dR/dT > 0$), also exhibiting SC up to the highest P (29 GPa) of this measurement. Above 12 GPa, T_c continues to increase only with marginal positive slope $dT_c/dP \sim 0.06$ K/GPa [Fig. 3(c)].

While releasing nonhydrostatic pressure, the normal metallic $R(T)$ is maintained down to 2 GPa and much to our surprise, the sharp SC transition is found to persist down to the lowest pressure (0.5 GPa), till the Pt lead remains in good pressure contacts with the sample [Fig. 3(d)]. Below 2 GPa, the normal state resistance above T_c displays unconventional metallic behavior, as was observed at 7 GPa during compression. At 0.5 GPa, SC onset $T_c \sim 3.2$ K and zero resistance is achieved at 1.6 K. Systematic lifting of this resistance drop under applied magnetic field further confirms the SC transition [33]. The irreversible nature and enhancement of T_c under decompression have recently been reported on layered chalcogenide compound In_2Se_3 [43]. This was attributed to the quenchable high-P phase (that hosts SC) as a result of 2D to 3D structural crossover, but eventually SC vanishes below 10 GPa as the system returns to the low-P phase. We report here that $1T$-$TiTe_2$ is the first compound to show the persistence nature of SC even after almost complete release of pressure. In quasihydrostatic decompression, SC vanishes below 5 GPa. Therefore the persistence nature of SC in $1T$-$TiTe_2$ can be attributed to structural irreversibility resulting from the nonhydrostatic compression. A detailed comparison of the structural behavior of $TiTe_2$ under hydrostatic [44] and nonhydrostatic pressures is given in the Supplemental Material [33].

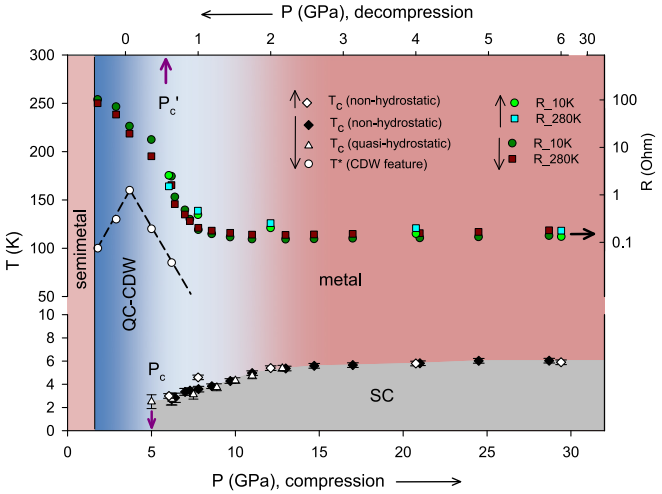

FIG. 4. The phase diagram for $1T$-$TiTe_2$ under nonhydrostatic compression (bottom P) and decompression (top P). Resistances at 10 and 280 K have been plotted on logarithmic scale (labels on the right axis, arrows in legends indicate corresponding scale). Top decompression P scale has been adjusted in order to match the T_c's and resistance values roughly with that of compression. P_c denotes onset pressure and zero resistance SC has been observed at P_c' upon decompression.

The results are summarized in the novel phase diagram of $1T$-$TiTe_2$ under nonhydrostatic compressions (Fig. 4). Although apparently the semimetallic state disappears above 1.8 GPa, a similar P variation of T_c as in the hydrostatic case suggests SC originating from the same semimetallic microstructure. Due to highly anisotropic axial compressibility, a drastic reduction in van der Waal interlayer spacing is observed, which probably helps CDW-like superstructures formation (having interdomain semimetallic undeformed regions) [33]. However, at elevated P the system becomes more isotropic, resulting in reduced deviatoric stress and so the CDW-like domains (or its coherence length) shrink in size and the semimetallic regions grow, responsible for the emergence of SC. A slightly higher critical pressure (6.2 GPa), compared to hydrostatic compression (where bulk semimetallic regions are present completely) further supports this explanation. This result is in disagreement with the real-space coexistence of CDW and SC as reported in $1T$-TaS_2 [15,19]. However, we cannot rule out the possibility of SC emerging from any hidden incommensurate CDW instability [14,20] that may be present in semimetallic state, which demands high-resolution structural investigation on the single crystal. The observed BCS nature of SC also hints at an enhanced electron-phonon coupling being the dominant mechanism for the formation of the CDW-like state. The slope change in SC T_c near 12 GPa can be associated with the structural transition to the $NbTe_2$-structured high-pressure phase [33], but demands a structural study below T_c for better understanding.

At much higher compression (for $P > 12$ GPa), the layered structure evolves into a 3D network (making Te-Te bonding between Te-Ti-Te layers) in an irreversible manner (as evidenced from reduced vdW gap at P release below 5 GPa), and so modifies the density of states at Fermi energy and phonon dispersion. The enhanced metallic character of the 3D network is maintained down to 2 GPa, where the T_c and resistance values are as per the extrapolated values from that above 12 GPa. Below 2 GPa, enhanced R in unconventional metallic regime and decrease of T_c indicate the existence of SC with reemergence of weak CDW-like order. Our electron diffraction study on this retrieved sample shows additional superstructure spots [33], evidencing possible CDW ordered phase at room temperature. As the SC volume fraction could not be measured on the retrieved sample, the filamentary nature of the recovered superconductivity cannot be ruled out. Further experiments on the P-released sample and theoretical calculations are required to fully understand the persistence nature of the superconductivity and reemergent CDW-like resistance anomaly.

In conclusion, pristine $1T$-$TiTe_2$ single crystals show pressure-induced SC transition above 5 GPa. Small nonhydrostatic P changes the T-dependence resistance drastically without affecting SC state, suggesting the emergence of phase-separated CDW-like domains within semimetallic regions. T_c continues to increase with P with a slope change at $\sim$12 GPa, where the structural property is believed to change from 2D to 3D character. Upon decompression from 29 GPa, the SC state persists down to 0.5 GPa where weak CDW order reappears, establishing a novel electronic phase diagram. Pressure-quenchable SC and its large upper critical field make $1T$-$TiTe_2$ a promising candidate for practical application. The decompression-driven observed pressure rescaling is of fundamental importance in layered SC, demanding further experimental and theoretical investigations. The present study also provides a unique opportunity to investigate a P-quenched SC sample for electronic structure by surface-sensitive techniques such as ARPES, ellipsometry, etc.

The authors thank N. Naveen Kumar and R. Tewari for providing the results of LEED measurements for characterizing the pristine and retrieved sample from nonhydrostatic compression study. Financial support by the Department of Science and Technology (Government of India) and ELETTRA Sincrotrone (Italy) are gratefully acknowledged.

[1] R. Klemm, *Layered Superconductors* (Oxford University Press, Oxford, UK, 2012), Vol. 1.

[2] F. Clerc, C. Battaglia, M. Bovet, L. Despont, C. Monney, H. Cercellier, M. G. Garnier, P. Aebi, H. Berger, and L. Forro, Phys. Rev. B **74**, 155114 (2006).

[3] K. Rossnagel, L. Kipp, and M. Skibowski, Phys. Rev. B **65**, 235101 (2002).

[4] T. E. Kidd, T. Miller, M. Y. Chou, and T.-C. Chiang, Phys. Rev. Lett. **88**, 226402 (2002).

[5] J.-P. Castellan, S. Rosenkranz, R. Osborn, Q. Li, K. E. Gray, X. Luo, U. Welp, G. Karapetrov, J. P. C. Ruff, and J. van Wezel, Phys. Rev. Lett. **110**, 196404 (2013).

[6] E. Morosan, H. W. Zandbergen, B. S. Dennis, J. W. G. Bos, Y. Onose, A. P. R. T. Klimczuk, N. P. Ong, and R. J. Cava, Nat. Phys. **2**, 544 (2006).

[7] J. F. Zhao, H. W. Ou, G. Wu, B. P. Xie, Y. Zhang, D. W. Shen, J. Wei, L. X. Yang, J. K. Dong, M. Arita *et al.*, Phys. Rev. Lett. **99**, 146401 (2007).

[8] S. Y. Li, G. Wu, X. H. Chen, and L. Taillefer, Phys. Rev. Lett. **99**, 107001 (2007).

[9] G. Wu, H. X. Yang, L. Zhao, X. G. Luo, T. Wu, G. Y. Wang, and X. H. Chen, Phys. Rev. B **76**, 024513 (2007).

[10] H. Barath, M. Kim, J. F. Karpus, S. L. Cooper, P. Abbamonte, E. Fradkin, E. Morosan, and R. J. Cava, Phys. Rev. Lett. **100**, 106402 (2008).

[11] R. Ang, Y. Tanaka, E. Ieki, K. Nakayama, T. Sato, L. J. Li, W. J. Lu, Y. P. Sun, and T. Takahashi, Phys. Rev. Lett. **109**, 176403 (2012).

[12] R. Ang, Y. Miyata, E. Ieki, K. Nakayama, T. Sato, Y. Liu, W. J. Lu, Y. P. Sun, and T. Takahashi, Phys. Rev. B **88**, 115145 (2013).

[13] Y. Liu, D. F. Shao, L. J. Li, W. J. Lu, X. D. Zhu, P. Tong, R. C. Xiao, L. S. Ling, C. Y. Xi, L. Pi *et al.*, Phys. Rev. B **94**, 045131 (2016).

[14] A. Kogar, G. de la Pena, S. Lee, Y. Fang, S.-L. Sun, D. Lioi, G. Karapetrov, K. Finkelstein, J. Ruff, P. Abbamonte *et al.*, Phys. Rev. Lett. **118**, 027002 (2017).

[15] S. Yan, D. Iaia, E. Morosan, E. Fradkin, P. Abbamonte, and V. Madhavan, Phys. Rev. Lett. **118**, 106405 (2017).

[16] C. S. Snow, J. F. Karpus, S. L. Cooper, T. E. Kidd, and T.-C. Chiang, Phys. Rev. Lett. **91**, 136402 (2003).

[17] B. Sipos, A. F. Kusmartseva, A. Akrap, H. Berger, L. Forr, and E. Tutis, Nat. Mater. **7**, 960 (2008).

[18] A. F. Kusmartseva, B. Sipos, H. Berger, L. Forró, and E. Tutiś, Phys. Rev. Lett. **103**, 236401 (2009).

[19] T. Ritschel, J. Trinckauf, G. Garbarino, M. Hanfland, M. v. Zimmermann, H. Berger, B. Bchner, and J. Geck, Phys. Rev. B **87**, 125135 (2013).

[20] Y. I. Joe, X. M. Chen, P. Ghaemi, K. D. Finkelstein, G. A. de la Pea, Y. Gan, J. C. T. Lee, S. Yuan, J. Geck, G. J. MacDougall, T. C. Chiang *et al.*, Nat. Phys. **10**, 421 (2014).

[21] B. Wang, Y. Liu, K. Ishigaki, K. Matsubayashi, J. Cheng, W. Lu, Y. Sun, and Y. Uwatoko, Phys. Rev. B **95**, 220501 (2017).

[22] S. Kawasaki, Y. Tani, T. Mabuchi, K. Kudo, Y. Nishikubo, D. Mitsuoka, M. Nohara, and G.-Q. Zheng, Phys. Rev. B **91**, 060510 (2015).

[23] M. Calandra and F. Mauri, Phys. Rev. Lett. **106**, 196406 (2011).

[24] R. Claessen, R. O. Anderson, J. W. Allen, C. G. Olson, C. Janowitz, W. P. Ellis, S. Harm, M. Kalning, R. Manzke, and M. Skibowski, Phys. Rev. Lett. **69**, 808 (1992).

[25] R. Claessen, R. O. Anderson, G.-H. Gweon, J. W. Allen, W. P. Ellis, C. Janowitz, C. G. Olson, Z. X. Shen, V. Eyert, M. Skibowski *et al.*, Phys. Rev. B **54**, 2453 (1996).

[26] Y. Koike, M. Okamura, T. Nakanomyo, and T. Fukase, J. Phys. Soc. Jpn. **52**, 597 (1983).

[27] D. K. G. de Boer, C. F. van Bruggen, G. W. Bus, R. Coehoorn, C. Haas, G. A. Sawatzky, H. W. Myron, D. Norman, and H. Padmore, Phys. Rev. B **29**, 6797 (1984).

[28] N. V. Baranov, V. G. Pleshchev, N. V. Selezneva, E. M. Sherokalova, A. V. Korolev, V. A. Kazantsev, and A. V. Proshkin, J. Phys.: Condens. Matter **21**, 506002 (2009).

[29] J. Khan, C. M. Nolen, D. Teweldebrhan, D. Wickramaratne, R. K. Lake, and A. A. Balandinc, Appl. Phys. Lett. **100**, 043109 (2012).

[30] R. C. Xiao, W. J. Lu, D. F. Shao, J. Y. Li, M. J. Wei, H. Y. Lv, P. Tong, X. B. Zhua, and Y. P. Sun, J. Mater. Chem. C **5**, 4167 (2017).

[31] Z. Zhu, Y. Cheng, and U. Schwingenschlögl, Phys. Rev. Lett. **110**, 077202 (2013).

[32] Q. Zhang, Y. Cheng, and U. Schwingenschlögl, Phys. Rev. B **88**, 155317 (2013).

[33] See Supplemental Material at http://link.aps.org/supplemental/10.1103/PhysRevB.97.060503 for synthesis, characterization by XRD, LEED, resistivity, and magnetic susceptibility on the as-grown sample as well as magnetoresistance, dc susceptibility on the pressurized sample, nonhydrostatic compression technique, high-pressure XRD, and LEED on the P-retrieved sample. This includes Refs. [45–48].

[34] J. Zabaleta, S. C. Parks, B. Baum, A. Teker, K. Syassen, and J. Mannhart, Rev. Sci. Instrum. **88**, 033901 (2017).

[35] Y. Guo, J. Dai, J. Zhao, C. Wu, D. Li, L. Zhang, W. Ning, M. Tian, X. C. Zeng, and Y. Xie, Phys. Rev. Lett. **113**, 157202 (2014).

[36] N. R. Werthamer, E. Helfand, and P. C. Hohenberg, Phys. Rev. **147**, 295 (1966).

[37] H. Suderow, V. G. Tissen, J. P. Brison, J. L. Martínez, and S. Vieira, Phys. Rev. Lett. **95**, 117006 (2005).

[38] V. G. Tissen, M. R. Osorio, J. P. Brison, N. M. Nemes, M. García-Hernández, L. Cario, P. Rodière, S. Vieira, and H. Suderow, Phys. Rev. B **87**, 134502 (2013).

[39] K.-H. Müller, G. Fuchs, A. Handstein, K. Nenkov, V. N. Narozhnyi, and D. Eckert, J. Alloys Compd. **322**, L10 (2001).

[40] X. Xi, Z. Wang, W. Zhao, J.-H. Park, K. T. Law, H. Berger, L. Forr, J. Shan, and K. F. Mak, Nat. Phys. **12**, 139 (2016).

[41] Y. Lu, T. Takayama, A. F. Bangura, Y. Katsura, D. Hashizume, and H. Takagi, J. Phys. Soc. Jpn. **83**, 023702 (2014).

[42] P. B. Allen and N. Chetty, Phys. Rev. B **50**, 14855 (1994).

[43] F. Ke, H. Dong, Y. Chen, J. Zhang, C. Liu, J. Zhang, Y. Gan, Y. Han, Z. Chen, C. Gao *et al.*, Adv. Mater. **29**, 1701983 (2017).

[44] V. Rajaji, U. Dutta, P. C. Sreeparvathy, S. C. Sarma, Y. A. Sorb, B. Joseph, S. Sahoo, S. C. Peter, V. Kanchana, and C. Narayana, Phys. Rev. B **97**, 085107 (2018).

[45] R. Pervin, M. Krishnan, A. K. Rana, M. Kannan, S. Arumugam, and P. M. Shirage, Phys. Chem. Chem. Phys. **19**, 11230 (2017).

[46] A. Dewaele, P. Loubeyre, and M. Mezouar, Phys. Rev. B **70**, 094112 (2004).

[47] A. Hammersley, *Computer Program FIT2D* (ESRF, Grenoble, 1998).

[48] A. C. Larson and R. B. von Dreele, Report No. LAUR 86-748, Los Alamos National Laboratory, New Mexico, 1986.